Research Square

Preprints are preliminary reports that have not undergone peer review.
They should not be considered conclusive, used to inform clinical practice,
or referenced by the media as validated information.

Climate teleconnection networks in Colombia

Nicole Rivera-Parra
Universidad de Antioquia
Isabel Hoyos
ichoyos@uniquindio.edu.co
University of Quindío
Francina Dominguez
University of Illinois Urbana-Champaign
Boris Rodríguez
Universidad de Antioquia

Research Article

Keywords: Climate Networks, Causal Teleconnections, Information Transfer, Tropical Andes Climate Dynamics, Climate Networks

Posted Date: October 13th, 2026

DOI: https://doi.org/10.21203/rs.3.rs-10935713/v1

License: This work is licensed under a Creative Commons Attribution 4.0 International License.
Read Full License

Additional Declarations: No competing interests reported.

Climate teleconnection networks in Colombia

Nicole Rivera-Parra[1], Isabel Hoyos[2], Francina Dominguez[3], Boris Rodríguez[1]

[1]Grupo de Fundamentos y Enseñanza de la Física y los Sistemas Dinámicos, Universidad de Antioquia, Calle 67 No. 53 – 108, Medellín, 050010, Antioquia, Colombia.
[2]Grupo de Física Teórica y Computacional, Universidad del Quindío, Carrera 15 Calle 12 Norte, Armenia, 630004, Quindío, Colombia.
[3]Department of Climate, Meteorology, and Atmospheric Sciences, University of Illinois at Urbana-Champaign, 1301 W. Green Street, Urbana, 61801, Illinois, United States.

Contributing authors: nicole.rivera@udea.edu.co; ichoyos@uniquindio.edu.co; francina@illinois.edu; boris.rodriguez@udea.edu.co;

Abstract

This contribution investigates the spatial and dynamic structure of climate teleconnections in Colombia by integrating complex network analysis with causal information-transfer flow methods. We examine the influence of six ocean-atmosphere coupled variability modes (Niño 3.4, Niño 3, SOI, TNA, NTA, and CAR) on three key regional climate variables: surface temperature, total precipitation, and vertical moisture flux convergence. Regional climate networks reveal heterogeneous connectivity patterns. The resulting networks display a hybrid structural complexity classification that does not conform to canonical statistical distributions. ENSO-related indices show a strong causal influence on precipitation and moisture flux over northern and western Colombia. In contrast, Atlantic indices exhibit significant but more spatially localized impacts over the Orinoco and Amazon basins. Notably, no significant causal influence is found between ENSO and surface temperature, suggesting a dominant influence from other climatic drivers. Unlike traditional correlation analysis, complex networks provide additional measures of centrality, closeness, and betweenness that highlight the regions critical for the transfer of information in the study area. Our findings highlight the central dynamic role of the Tropical Andes in shaping

regional climate connectivity and network betweenness. This framework provides new insights into the spatial organization of climate variability and offers a complementary toolset for regional information-based techniques.

Keywords: Climate Networks, Causal Teleconnections, Information Transfer, Tropical Andes Climate Dynamics, Climate Networks

1 Introduction

Colombia exhibits pronounced climatic and environmental complexity, arising from the interaction of atmospheric transport processes, climate variability, biodiversity, and ecohydrological processes (Myers et al. 2000; Bass et al. 2010; Sánchez-Cuervo et al. 2012; Aldana-Domínguez et al. 2017; Arias et al. 2021). The country's hydroclimate reflects the combined effects of global climate modes, regional circulation patterns, and complex local orography, influenced by climate variability originating in both the Pacific and Atlantic basins and strongly modulated by the migration of the Intertropical Convergence Zone. These interactions generate marked spatio-temporal variability in precipitation, temperature, and climate fields across multiple scales (Mesa S et al. 1997; IDEAM 2005; Poveda et al. 2011; Hoyos et al. 2013, 2018, 2019; Urrea et al. 2019; Pabón-Caicedo et al. 2020; Espinoza et al. 2020), challenging the disentanglement of the relative contributions, mechanisms, and spatial footprints of dominant variability sources, which is likely intensified under climate change (Lee et al. 2023).

Correlation-based analyses, regression methods, and composite approaches are among the most common methods to establish climate teleconnections (Wilks 2019). While these methods have yielded valuable insights, they often rely on linear assumptions, focus on pairwise relationships, and struggle to capture the multivariate, nonlinear, and spatially distributed nature of climate interactions. In regions such as Colombia, where multiple drivers coexist and interact with steep topography, these limitations hinder a comprehensive representation of teleconnection structures and their dynamical pathways.

Complex network theory is a powerful alternative framework for characterizing climate connectivity by identifying the most important associations among spatial points (Tsonis and Roebber 2004; Deza 2015; Donner et al. 2017; Dijkstra et al. 2019). In climate networks, nodes correspond to spatial locations, while links encode statistical or causal relationships between climatic variables connecting nodes that are quantified by specific metrics (Tsonis and Roebber 2004; Tsonis et al. 2006, 2008; Fortunato 2010; Newman et al. 2011). The resulting network topology provides a compact representation of the underlying interaction structure and facilitates the identification of key regions, pathways, and spatial patterns of influence (West and Scafetta 2010; Deza and Ihshaish 2015; Dijkstra et al. 2019). Recent studies have

successfully applied this approach in South America to investigate the climate modulation of large-scale modes such as the El Niño–Southern Oscillation (Rehbein and Ambrizzi 2023) and the impacts of climate variability on hydrological and biogeochemical processes (Rehbein and Ambrizzi 2023; Serrão et al. 2025).

In this study, we investigate the structure of global-driven climate teleconnections over Colombia using a network-based framework in which climate links are established from information-based causal analysis, which performs better than classical correlation analysis Docquier et al. (2024). This framework enables the identification of dominant connectivity patterns due to global climate variability that shape the Colombian hydroclimate variability. The resulting networks exhibit hybrid topological architectures that do not fully conform to canonical network taxonomies; nevertheless, they reveal spatially organized connectivity patterns consistent with known teleconnection mechanisms and highlight the role of the Colombian Andes in modulating regional climate interactions.

2 Study area and Data

This study examines climate connectivity in northern South America, with a focus on Colombia (Figure 1). In this region, the orographical complexity of the Andes mountain range shapes the atmospheric dynamics and regional climate patterns (Poveda et al. 2006; Espinoza et al. 2020; Poveda et al. 2020). The resulting landscape comprises a mixture of ecosystems, including moist rainforests, grasslands, high mountains, dry forests, deserts, and mangroves, which provide a wide range of ecosystem services (Díaz-Granados Ortiz et al. 2005; Sánchez-Cuervo et al. 2012; Aldana-Domínguez et al. 2017).

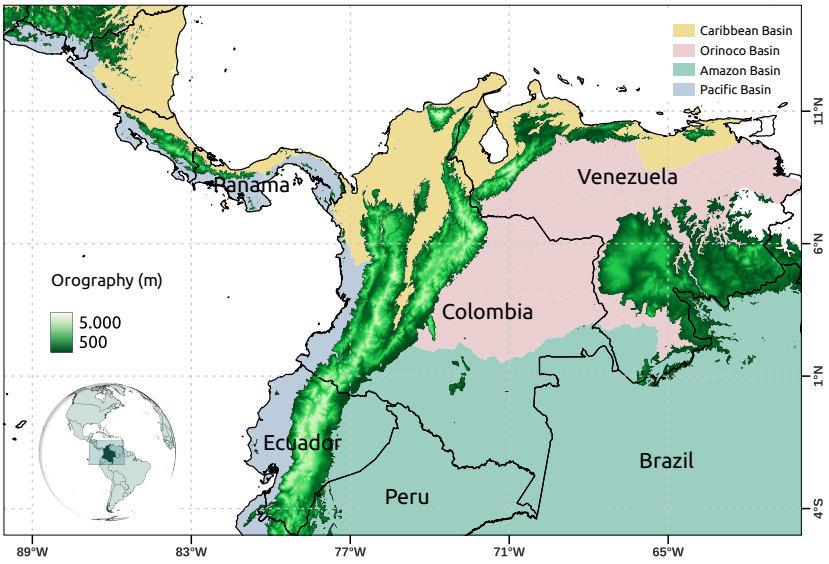


Fig. 1 Study area. The target region focuses on northern South America, centered on Colombia.

The spatial structure of rainfall and climate classification is mostly defined by the interaction of the Intertropical Convergence Zone (ITCZ), regional transport phenomena, and regional orography (Poveda et al. 2006, 2011; Urrea et al. 2019; Pabón-Caicedo et al. 2020; Escobar et al. 2022). Sources of regional climate variability combine effects from Pacific and Atlantic oceanic (or land-sea coupled) modes, operating at multiple spatio-temporal scales (Poveda et al. 2006, 2011; Hoyos et al. 2013, 2018, 2019; Espinoza et al. 2020; Arias et al. 2023; Builes-Jaramillo et al. 2023; Duque-Gardeazabal et al. 2024; Ruiz-Vásquez et al. 2024), such as El Niño Southern Oscillation (ENSO), the Tropical Northern and Southern Atlantic (TNA and TSA), North Tropical Atlantic (NTA), Caribbean Sea (CAR), Atlantic Meridional Mode (AMM), Atlantic Multidecadal Oscillation (AMO), Pacific Meridional Mode (PMM), and Pacific Decadal Oscillation (PDO), among others.

In agreement with the IPCC Sixth Assessment Report (Lee et al. 2023), increasing temperatures and shifting precipitation patterns are expected in this region, leading to more frequent extreme events and threatening key sectors in Colombia, such as coffee production (Sanderson et al. 2022). Food security and agricultural activities highly rely on the nation's capability to predict and manage extremes (Botero and Barnes 2022). Further, 68% of the country's electricity depends on hydroelectric power; consequently, the intensification of droughts and rainfall is a potential risk to national energy security.

In this work, the regional climate state is summarized by three key monthly variables: total precipitation (TP), two-meter temperature (T2M), and vertically

integrated moisture flux convergence (VIMF). Data are provided by ERA5 reanalysis in a spatial resolution of 0.25° for the period from 1950 to 2020 (Hersbach et al. 2020a,b). Six global modes of leading regional variability of atmospheric processes were selected based on findings from Hoyos et al. (2018) and Hoyos et al. (2019), as specified in Table 1. Indices are sourced from the NOAA repository (https://psl.noaa.gov/data/climateindices/list/).

Table 1 Global modes of variability influencing regional atmospheric processes.

Variability mode (index)	Variability time-scale
Tropical Pacific: El Niño Southern Oscillation (Niño 3/Niño 3.4/SOI)	Interannual
SST in the Tropical Caribbean/Atlantic (CAR/NTA)	Monthly to annual
SST in the Tropical Northern Atlantic (TNA)	Monthly to annual

3 Methods

The present analysis builds on the climate-network framework (Deza and Ihshaish 2015; Donges et al. 2015; Donner et al. 2017; Dijkstra et al. 2019). Following the categorization proposed by Froyland et al. (2014) and Donges et al. (2015), climate networks can be grouped into three types: (i) functional networks, constructed through linear or nonlinear correlation measures such as cross-correlations or mutual information; (ii) flow networks, derived from the analysis of transport processes within dynamical flows; and (iii) event-synchronization networks, which arise from examining correlations and time delays associated with extreme events. In this study, we adopt the functional-network approach, incorporating a connectivity metric based on the scale of information flow from time series representing specific modes of global climate variability to time series characterizing local climate states. Nodes correspond to a regular spatial grid covering a square region centered on Colombia, with each node representing a 0.25° grid cell (see Appendix A for the grid-cell–node correspondence). The squared $N \times N$ Adjacency Matrix $A = \{a_{ij}\}$, represents the linking from node j to node i.

Selecting appropriate quantifiers to define the links within the network is crucial, as the connections determine the network's topological structure (Xu 2001). Some traditional criteria for defining links in climate networks are geographic distance, climate correlations, or relevant statistics (Boccaletti et al. 2006; Donner et al. 2009; Steinhaeuser et al. 2010; Deza and Ihshaish 2015; Donner et al. 2017). Considering that the probability density function provides a statistical representation of access to climatic phase space, whereas transition probabilities arise from dynamic interactions among components (Jönsson et al. 2023), we include a causal quantifier involving asymmetric information transfer flow for establishing the linking structure of variability climate networks.

3.1 Information-based causal links

The Liang-Kleeman formalism introduces a quantifier for the information transfer rate between two time series $X(t)$ and $Y(t)$ (Liang 2014, 2016; Tawia Hagan et al. 2019). Consider the composed system $\boldsymbol{S} = \{X(t), Y(t)\}$ follows the simplest bi-dimensional stochastic-dynamic

$$\frac{d\boldsymbol{S}}{dt} = \boldsymbol{F} + \boldsymbol{B}\frac{d\boldsymbol{W}}{dt}, \tag{1}$$

where $\boldsymbol{F} = \boldsymbol{f} + \boldsymbol{M}\boldsymbol{S}$ accounts for the linear deterministic dynamics, being $\boldsymbol{f} = (f_1, f_2)^T$ and $\boldsymbol{M} = (m_{ij})$ the coefficient matrix. $\boldsymbol{W}$ accounts for a standard Wiener process with $\boldsymbol{B}$ a diagonal matrix of b_1 and b_2 values (Majda and Harlim 2007; Liang 2014; Lozano-Durán and Arranz 2022). The Liang-Kleeman information flow (LKIF) for the rate of information flowing from the state variable Y to X is

$$T_{Y\to X} = \frac{C_{XX}C_{XY}C_{Y\dot{X}} - C_{XY}^2 C_{X\dot{X}}}{C_{XX}^2 C_{YY} - C_{XX}C_{XY}^2}. \tag{2}$$

C_{ij} is the sample covariance between the time series of processes X and Y, and $\dot{}$ represents the time derivative. This asymmetric measure is given in units of nats/time and distinguishes the direction of information flow. Following the principle of nil causality, $T_{Y\to X} = 0$ indicates independence between time series. A nonzero $T_{Y\to X}$ can be either positive or negative. A negative value means Y makes X more predictable by restricting its accessible states, while a positive value means Y indeterminates X by expanding its accessible state space. In the context of dynamical systems, a source of uncertainty is understood as a dynamic variable whose small variations significantly increase the number of possible states that another variable can take. $T_{Y\to X}$ bridges classical determinism and stochasticity by including a comprehensive concept of causality (Majda and Harlim 2007; Liang 2018; Lozano-Durán and Arranz 2022). Further detailed mathematical demonstration is provided in Liang (2008, 2014, 2016, 2018).

A normalized LKIF (Liang 2015) considers that the evolution of marginal entropy of X ($Z_{Y\to X}$) is composed of stochastic effects (H_X^{noise}), self-driven changes in X (dH_X^*), and the information flow from Y to X ($T_{Y\to X}$), as

$$Z_{Y\to X} \equiv \left|\frac{dH_X^{noise}}{dt}\right| + \left|\frac{dH_X^*}{dt}\right| + |T_{Y\to X}|. \tag{3}$$

Since $|Z_{Y\to X}| \geq |T_{Y\to X}|$, the relative contribution to information flow is

$$\tau_{Y\to X} = \frac{T_{Y\to X}}{Z_{Y\to X}}. \tag{4}$$

$|\tau_{Y\to X}| = 1$ (or 100%) if the change in information content of X is entirely due to Y. Conversely, $\tau_{Y\to X} = 0$ implies no causal influence from Y, which is useful to reveal the relative importance of a causal relationship among processes (Liang 2015; Takaya et al. 2025).

Common features in information transfer are understood as a property of universality underlying the microscopic states of the atmospheric organization, as in complex or critical phenomena (Stanley 1999; Hoyos and Rodríguez 2020; Sethna 2021). In our model, nodes i and j are linked if they received the same relative information transference for a given global climate index h and a local climate variable k. A two-sided significance level of 0.5% indicates that a value of $|0.005|$ is the minimum threshold of detectable dynamical influence, establishing the resolution in the scale of τ. Consequently, $\tau_{2\to1} \in (-0.005, 0.005)$ is set as zero. The elements of the adjacency matrix A for a particular index h are defined as

$$a_{ij}^{(h)} = \begin{cases} 1, & \text{if } \mid \tau_{h\to k}^{i} - \tau_{h\to k}^{j} \mid < 0.005;\ \forall k \text{ and } \forall \tau \neq 0 \\ 0, & \text{otherwise} \end{cases}. \tag{5}$$

These adjacency matrices are symmetric, unweighted, and undirected. Diagonal elements are set to zero because this analysis focuses on inter-location relationships.

3.2 Network's properties

Structural and functional network features are determined through a set of key properties such as graph density, degree, clustering coefficient, network entropy, distances, eccentricities, and graph diameter and radius. These properties collectively describe resilience, compactness, and efficiency of networks, which are crucial in evaluating network behavior in the framework of complexity (Newman 2002; Barrat et al. 2008; Cohen and Havlin 2010; Newman et al. 2011; Barabási and Pósfai 2016; Donner et al. 2017). The definitions, symbols, and mathematical formulations for each property are presented in Table 2.

Centrality measures such as degree centrality, closeness, betweenness, and eigenvector centrality play a key role in characterizing nodes within the network, particularly in identifying spatial patterns of climate connectivity.

Closeness centrality quantifies a node's efficiency in reaching others by calculating its mean geodesic distance to all other nodes; nodes with high closeness values exhibit greater accessibility across the network. Betweenness centrality measures how often a node lies on the shortest paths between pairs of nodes, highlighting its role in facilitating interconnections among different network regions. These metrics offer a detailed understanding of the network's structure and information flow pathways, providing insights into teleconnection patterns within the study area (Newman 2018; Golbeck 2015). Eigenvector centrality extends degree centrality by assigning greater importance to nodes that are connected to other highly central nodes, thereby highlighting influential hubs within the network (Negre et al. 2018).

Table 2 Network Properties and Definitions, based on Newman (2018), Barabási and Pósfai (2016), Cohen and Havlin (2010), and Barrat et al. (2008).

Property	Formula	Description
Node degree	$k_i = \sum_j a_{ij}$	Number of links at a given node
Network density	$\mathcal{D} = \frac{2L}{N(N-1)}$	Ratio between actual links and possible links, indicating connectivity
Distance between nodes	$d_i = \min d_{i,j}$	Shortest path link count between nodes i and j
Node eccentricity	$\epsilon_i = \max d_{i,j}$	Greatest shortest path distance from node i to any other node
Local clustering coefficient	$C_i = \frac{1}{k_i(k_i-1)} \sum_{jk} a_{ij} a_{jk} a_{ki}$	Likelihood of node i's neighbors being interconnected
Network entropy	$\mathcal{H} = \frac{1}{N \log(N-1)} \sum_{i=1}^{N} \log k_i$	Measure of network degree distribution heterogeneity
Radius	$\mathbf{R} = \min \epsilon_i$	Smallest maximum shortest path distance from any node
Diameter	$\mathbf{D} = \max \epsilon_i$	Longest shortest path in the network

4 Results and Discusion

4.1 Source of climate variability

Figure 2 compares the influence and relative importance of ENSO (Niño3.4 index) on the regional climate state, as represented by correlation, LKIF, and normalized LKIF. Negative LKIF values capture spatial patterns similar to those identified through correlation. In contrast, positive LKIF values reveal regions that are not significantly correlated with ENSO but remain causally connected. In these regions, ENSO reduces the predictability of climate variability by weakening deterministic relationships and enhancing stochastic variability. The normalized LKIF further indicates that the relative contribution of ENSO to climate variability is spatially targeted.

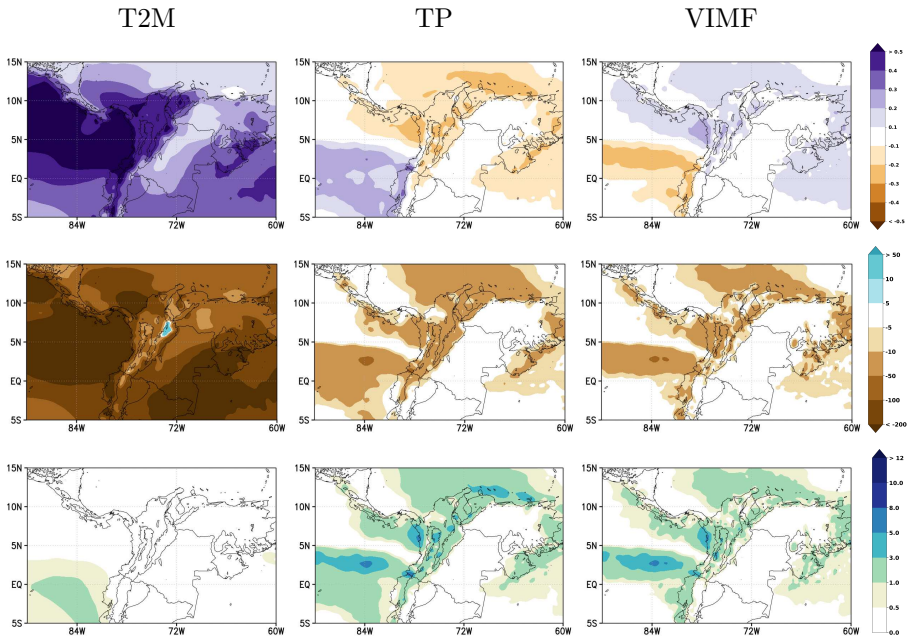


Fig. 2 Influence of ENSO-Niño3.4 index on T2M, TP, and VIMF measured by correlation (top row), LKIF (middle row, in milinats per month), and normalized LKIF (bottom row, in %).

For T2M (TP and VIMF) variability, the relative influence of ENSO is weaker and more spatially diffuse (stronger and more localized) than suggested by correlation, particularly over mountainous regions. ENSO exhibits its strongest causal influence on Colombian TP. Normalized LKIF is predominantly negative over the eastern equatorial Pacific cold tongue, western Colombia, the Pacific boundary of Central America, the Caribbean region, the Colombian inter-Andean valleys, and the northern Amazon, indicating that ENSO constrains precipitation uncertainty in these areas. The spatial causal structure of VIMF is similar to, though weaker than, that of TP across ENSO indices, suggesting that both precipitation and vertical moisture flux convergence are strongly influenced by ENSO in key regions. This behavior is consistent with previous studies emphasizing the role of the Pacific in modulating regional hydroclimatic variability (Hoyos et al. 2019; Cai et al. 2020; Posada-Marín et al. 2023).

Similar qualitative results are obtained for Niño3 and the SOI index (see Appendix B2 and B3). However, the latter exhibits a more pronounced effect in increasing the unpredictability of TP and VIMF variability over southeastern Colombia, suggesting localized interactions distinct from those associated with the other ENSO indices. Despite these differences across indices, the overall ENSO influence on TP remains consistent. In this context, the relationship between ENSO and TP provides a clear representation of tropics–tropics teleconnections, consistent with precipitation deficits (excess) during El Niño (La Niña) events over northern South America (Kousky et al. 1984; Souza and Ambrizzi 2002; Waylen and Poveda 2002; Poveda et al. 2006; Grimm

and Tedeschi 2009; Arias et al. 2015; Cordoba-Machado et al. 2015; Cai et al. 2019; Hoyos et al. 2019; Canchala et al. 2020; Ruiz-Vásquez et al. 2024).

In contrast, the teleconnections associated with the Atlantic variability are comparatively weaker across the study area. Figure 3 shows the Atlantic influence (TNA index) on the regional climate state. Atlantic variability exhibits a causal–correlated influence on regional T2M with respect to the TNA index. Positive LKIF values indicate that TNA primarily acts as a source of causal indeterminacy; however, the normalized LKIF shows that its relative contribution to regional T2M variability barely reaches 1%, and is spatially localized over the Andean and inter-Andean regions of Colombia and Ecuador, as well as eastern Venezuela. TP exhibits weak regional correlation, while positive LKIF values reveal causal indeterminacy over the southeastern corner, with a very low relative contribution to regional variability (less than 1%). The spatial structure of VIMF correlation contrasts with that of TP, but remains weak overall. In this case, causation is predominantly deterministic and localized over the northernmost Andes, although its relative contribution to explaining variability is also low. The NTA and CAR indices were also analyzed (see Appendix B4 and B5). The influence of NTA on the regional climate state follows the spatial structure identified for the TNA index, with consistent patterns in both correlation and LKIF. CAR exhibits a comparatively weaker influence, as indicated by lower LKIF values and a negligible contribution in normalized LKIF, suggesting a limited role in explaining regional variability.

In general, Atlantic and Pacific variability modes exhibit a weak causal influence on TP and VIMF over the Orinoco and Amazon foothills of the eastern mountain range. These results are consistent with findings from Hoyos et al. (2018) and Escobar et al. (2022), which indicate that moisture variability in the area is predominantly governed by local recycling processes rather than external climate forcing.

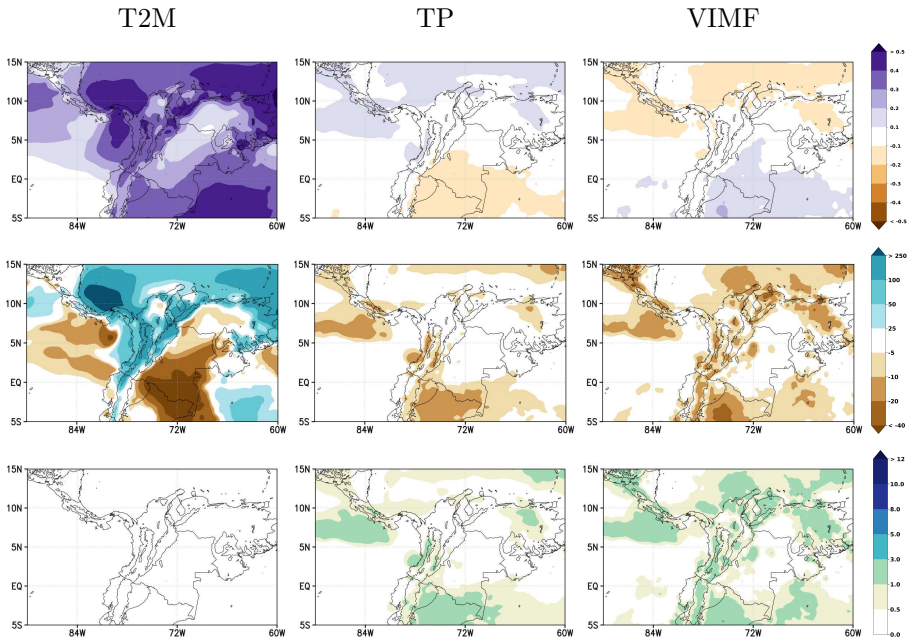


Fig. 3 Influence of TNA index on T2M, TP, and VIMF measured by correlation (top row), LKIF (middle row, in milinats per month), and normalized LKIF (bottom row, in %).

Table 3 summarizes the effects on regional climate combining correlation, LKIF, and normalized LKIF.

4.2 Regional climate networks

The study area is represented by a total of 9801 grid cells, which establishes the maximum number of possible connected nodes. The causal spatial interconnection structure for climate variability related to each global climate variability mode, as represented by TP, T2M, and VIMF state variables, is depicted by simple, undirected, and unweighted networks. Topological features of the climate networks for each index are summarized by the network's properties (Table 4) and their corresponding node degree distributions (Fig 4). For visualizing the adjacency matrices, see Appendix C.

Large networks were obtained, comprising more than 2,000 nodes and over one million links. However, the percentage of connected spatial points varies between 64.11% and 26.45% across the different indices, revealing a sparse regional climate connection structure. This sparsity highlights the heterogeneous spatial distribution of teleconnection patterns driven by the different modes of climate variability and suggests the presence of distinct mechanisms of information transfer or causal influence. Furthermore, the total number of connected nodes, N, can be interpreted as an indicator of the proportion of the study area dynamically influenced by each index, ranked as follows: Niño 3.4 (64.11%), TNA (59.18%), Niño 3 (55.55%), SOI (48.10%),

Table 3 Summary of indices effects on regional climate variability combining correlations, and information transfer analysis

Variability mode	T2M	TP/VIMF
Tropical Pacific interannual variability (ENSO)	T2M response is more predictable under ENSO, but with low relative causal influence across the area. High positive correlation indicates ENSO positive (negative) phase coincides with an increase (decrease) in regional temperature anomalies.	ENSO deterministically controls regional PP and VIMF. Negative (positive) correlation over western Colombia, the Caribbean, the inter-Andean mountain range, and northern Amazon (oceanic region beyond the Ecuadorian coast) indicates a decrease (increase) in precipitation during positive (negative) ENSO phases. VIMF shows an opposite correlation spatial structure, exhibiting an excess (deficit) of atmospheric vapor when rainfall experiences reduction (increase) under ENSO.
Tropical Atlantic and Caribbean Sea interannual variability	Positive correlation is not causally explained. A strong differentiated spatial pattern in LKIF shows that T2M in the Northern Andes and Caribbean Sea (Pacific Ocean and Northern Amazon) becomes more unpredictable (predictable) due to Atlantic variability, but it explains less than 1% of regional variability.	PP and WIMF exhibit low correlation with opposite patterns. Atlantic modes causally explain 3% of the PP and VIMF variability. LKIF detects deterministic influence over the Andes that correlations do not detect.

Table 4 Summary of climate network properties.

Network	N	L	$\langle k \rangle$	$\mathcal{D}$	$\langle \epsilon \rangle$	$\langle C \rangle$	$\mathcal{H}$	**R**	**D**
Niño 3.4	6238	8706501	1776.7	0.4412	3.119	0.705	0.545	3	5
Niño 3	5444	5234314	1068.1	0.3533	3.028	0.690	0.448	2	4
SOI	4714	5940966	1212.3	0.5348	3.805	0.769	0.402	3	6
TNA	5800	9961331	2032.7	0.5923	2.458	0.795	0.517	2	4
CAR	3846	3871346	790.0	0.5236	2.875	0.833	0.319	2	3
NTA	2592	1374263	280.4	0.4092	3.223	0.781	0.195	2	4

CAR (39.25%), and NTA (26.45%).

Network density $\mathcal{D}$ reveals a moderate level of regional climate connectedness, expressing a balance between the information flow and redundancy across the network. TNA expresses the highest degree of density, with nearly 60% of the maximum number of links that the network could have, while Niño 3 is the sparsest network with just 35%.

Average eccentricity $\langle \epsilon \rangle$ indicates that the maximum number of links needed to connect any two nodes is between 3 and 4 among networks, suggesting the presence of shortcuts and complex network structure, where emerging pathways reduce spatial distances in terms of shared information transfer related to global variability phenomena. The radius **R** (and diameter **D**) further support this result, with maximum

(minimum) network eccentricities ranging between 3 and 6 (2 and 3) links across all indices.

All networks exhibit a high clustering coefficient $\langle C \rangle$, confirming a modular network structure which can be visualized in the adjacency matrices (Fig. C6). This clusterization indicates minimized average distances between nodes, consistent with the compactness previously inferred from the network's eccentricity.

The degree distribution describes the probability p_k that a randomly selected node has degree k, and it is a useful metric for characterizing network complexity. As shown in Fig 4, the Niño 3.4, Niño 3, SOI, and TNA networks exhibit a high likelihood of hyper-connected nodes. These nodes work as key connectivity hubs within the networks, a role that will be further examined using centrality measures applied to each network's nodes. The ocean-driven climate variability connectivity in Colombia exhibits high clustering and low eccentricity (features characteristic of small-world networks) as well as hub regions indicative of preferential attachment (a hallmark of scale-free networks). However, none of the observed distributions conform to canonical forms such as the power law or Poisson distribution, suggesting a unique structure with mixed complexity.

In this context, network entropy $\mathcal{H}$ is a meaningful metric for capturing variability in the degree distribution. For Niño 3.4, Niño 3, SOI, and TNA, the average network entropy is approximately 0.5, indicating a balanced structure —neither sparse nor fully connected—without dominant peaks or tails. In contrast, CAR and NTA exhibit lower values of network entropy, in agreement with a flatter or peaked degree distribution (Fig. 4).

4.3 Centrality analysis

The degree centrality, closeness, and betweenness measures allow the identification of key spatial nodes and regions of high connectivity within the study area. Figure 5 illustrates the degree centrality for the six constructed networks. The networks associated with ENSO-related indices exhibit similar spatial patterns, characterized by a high level of centrality over the Caribbean region, Central America, and the Pacific Cold Tongue zone. Notably, Niño 3.4 and Niño 3 also display pronounced centrality over southern Venezuela and northern Brazil. The Inter-Andean region exhibits localized high centrality spots.

In contrast, the TNA, NTA, and CAR indices reveal distinct structural configurations. The highest degree centrality values for TNA are observed along the southern coast of Costa Rica and within the western Amazon rainforest in Brazil. CAR exhibits multiple connectivity spots distributed across the Colombian Andes, particularly within the Orinoco Basin near the eastern branch, as well as in northwestern Brazil. Among all indices, NTA presents the lowest overall degree centrality, with its primary

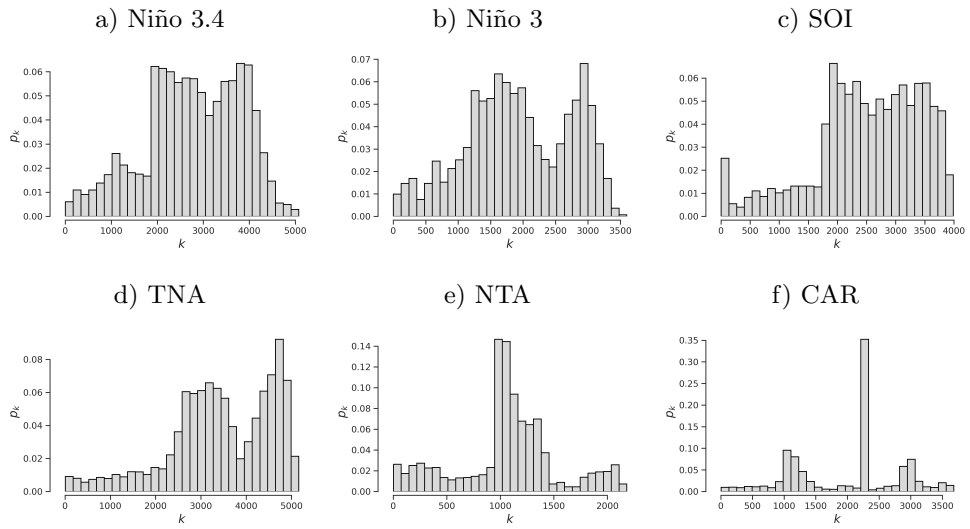


Fig. 4 Degree distribution for a) Niño 3.4, (b) Niño 3, (c) SOI, (d) TNA, (e) NTA, and (f) CAR indices.

area of influence concentrated in the valleys adjacent to the Colombian Andes.

Closeness centrality quantifies a node's ability to reach all other nodes in the network through the shortest paths, identifying both well-connected regions and those that are relatively isolated. Figure 6 shows the spatial distribution of closeness centrality for the six networks, indicating the relative proximity of each location to the rest of the study area based on causal connections mediated by teleconnections with the corresponding indices. In this visualization, darker regions denote nodes with higher closeness centrality, i.e., more central or proximal within the network. In contrast, lighter areas indicate nodes that are more peripheral or distant from others.

The Andean region consistently appears as a highly central area in the networks associated with Niño 3.4, Niño 3, SOI, and TNA, suggesting that it works as an efficient hub for the propagation of ocean-atmosphere teleconnection signals across Colombia and neighboring territories. In contrast, the CAR network highlights the Orinoco Basin as a region of high centrality, while the NTA network shows a more dispersed structure with moderate centrality values and fewer clearly defined central zones. These spatial patterns provide insights into the differentiated influence of each oceanic index on the continental climate dynamics, with potential implications for regional climate predictability and early warning systems.

Betweenness centrality identifies nodes that serve as critical intermediaries along shortest paths between other nodes, highlighting their structural significance in maintaining the network's overall cohesion. Figure 7 depicts the spatial distribution of

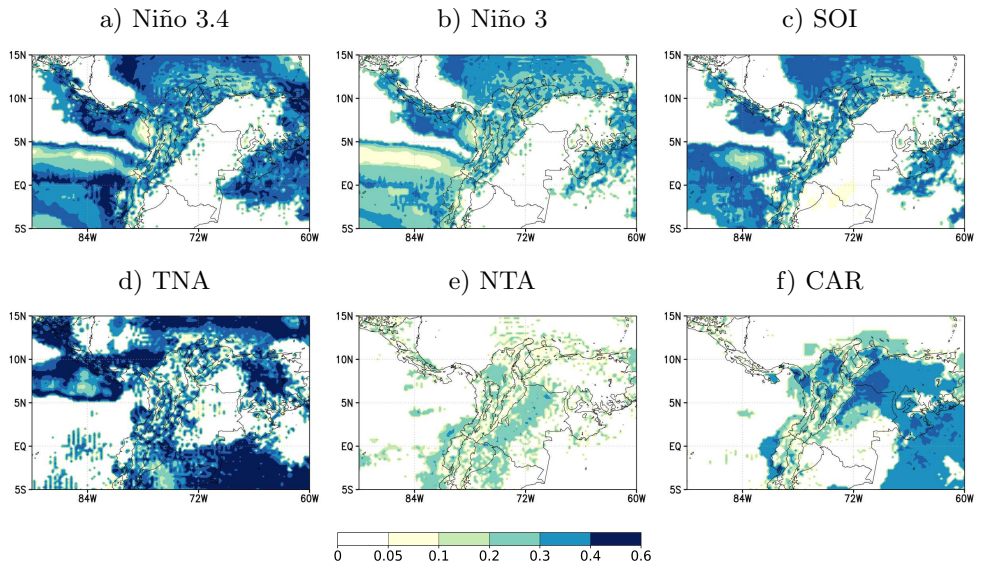


Fig. 5 Degree centrality maps. Higher degree values indicate greater connectivity within the network.

betweenness centrality across the six networks. The disconnection of nodes of higher structural importance would substantially alter the network's shortest path structure and, consequently, its overall eccentricity.

For the ENSO-related indices, the betweenness centrality patterns closely mirror those observed in the degree and closeness centrality measures. The Colombian Andes is a critical structural backbone, underscoring their consistent role in mediating climate teleconnections across the region. These findings emphasize the Andes' influence as a geographical hub within the climate network, potentially enhancing regional predictability associated with ENSO variability.

The TNA network exhibits moderately high betweenness values over the northwestern Amazon and the eastern Pacific near Panama and Costa Rica. Although these nodes are not the most structurally central in the broader network, their elevated centrality suggests a notable reliance on Amazonian connectivity to maintain the integrity of the teleconnection structure associated with this index. In the NTA network, structurally important nodes are distributed along the northern Andes and the adjacent Orinoco region, reinforcing the role of this mountainous corridor in shaping regional climate linkages. In the CAR network, the highest betweenness centrality values are concentrated in the Orinoco Basin, particularly near the Colombian–Venezuelan border. This suggests that the region works as a critical channel for the transmission of teleconnection signals between Colombia and the Caribbean.

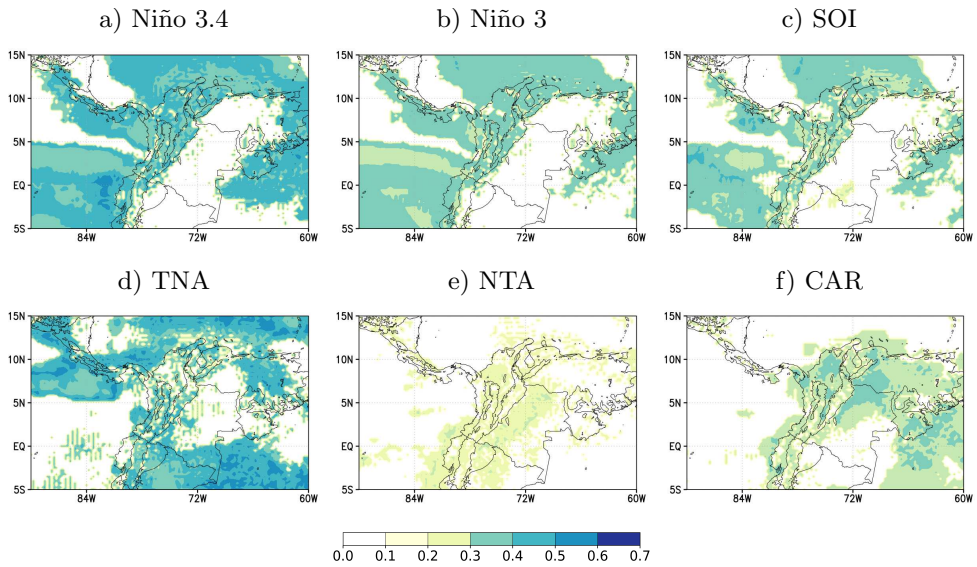


Fig. 6 Closeness centrality maps.

These measures consistently highlight the Colombian Andes as a prominent hub across most networks, particularly for ENSO-related indices and TNA. This region emerges as a recurrently central area, underscoring its strategic geographic and climatic position in the propagation and mediation of teleconnection signals.

Conversely, the CAR and NTA networks exhibit structurally distinct patterns. For CAR, the Orinoco Basin, especially near the Colombian–Venezuelan border, plays a critical structural role, while the NTA network reveals scattered centrality with peaks along the northern Andes and adjacent basins. The Amazon Basin, though largely isolated in the CAR and ENSO-related networks, exhibits localized centrality in the TNA network, suggesting a regionally constrained but potentially significant interaction between the Amazon and the tropical North Atlantic. This raises important questions about the influence of Atlantic variability on continental hydrological and atmospheric dynamics, especially over the Amazon and its periphery.

These zones of high spatial connectivity define hubs in the networks, which can also be identified in the maps of eigenvector centrality shown in Appendix D.

5 Concluding remarks

Climate network analysis offers a powerful framework for characterizing the dynamic influence of global climate phenomena on Colombia. It addresses the canonical question of climate teleconnections through an innovative lens aligned with the concept

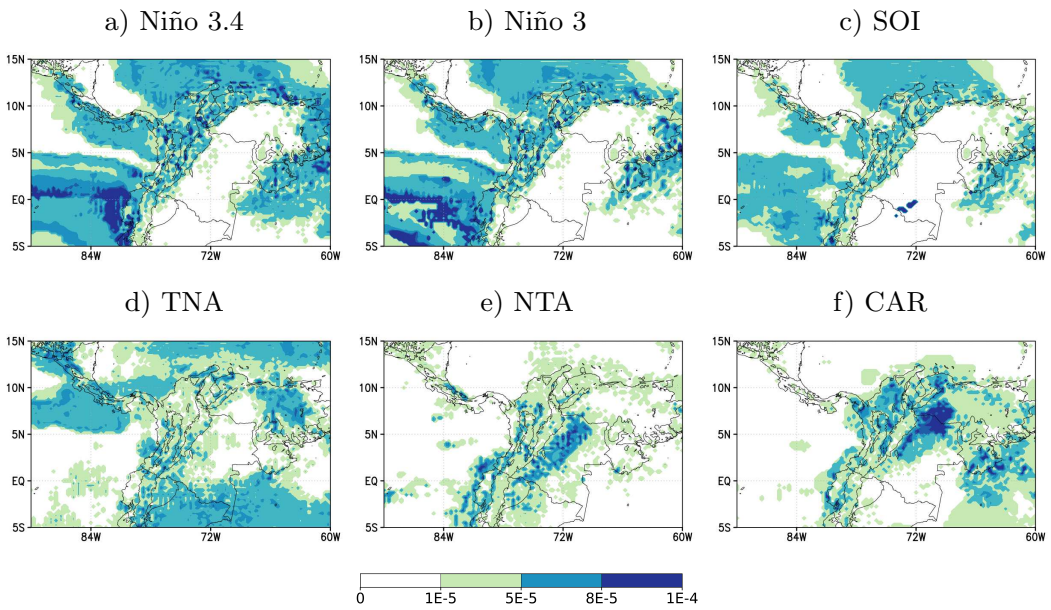


Fig. 7 Betweenness centrality maps. Higher values indicate higher structural importance.

of *network thinking*, in which the dynamics of nodes and links reveal critical insights into the location, intensity, and topology of climate influences. The application of the Liang-Kleeman estimator to quantify the rate of information flow from distinct global variability modes to regional climate states proves especially advantageous, dynamically uncovering nontrivial teleconnection patterns that may remain hidden in traditional correlation-based approaches.

Based on the estimated rates of information flow, we delineate the detailed spatial structure of the influence exerted by global climate variability modes on the climate state of Colombia and surrounding regions. ENSO is the dominant driver of precipitation variability (and likewise of moisture flux convergence), particularly through the Niño 3 and Niño 3.4 indices, exerting a strong and spatially coherent causal influence on precipitation patterns across northern, western, and northwestern Colombia, as well as the inter-Andean zone. The Andean mountain range appears to act as a geographic boundary limiting the eastward extent of ENSO's causal influence. These findings are consistent with the spatial organization of teleconnections reported in previous studies, such as Kousky et al. (1984); Aceituno (1988); Souza and Ambrizzi (2002); Poveda et al. (2006); Grimm and Tedeschi (2009); Cai et al. (2020); Ruiz-Vásquez et al. (2024).

Atlantic variability modes exert a weaker overall influence on the target region compared to Pacific modes. Nevertheless, they are causally linked to rainfall variability in eastern and southeastern Colombia, with notable effects over the Orinoco

and Amazon basins (as discussed in Duque-Gardeazabal et al. (2024)). These results highlight the important but regionally distinct role of the Atlantic Ocean in shaping Colombian climate teleconnections.

Pacific and Atlantic variability modes exhibit only a minor causal influence on surface temperature compared to other sources of information flow. This suggests that other climatic processes, possibly of local or continental origin, may be responsible for modulating temperature variability in Colombia. Tsonis and Swanson (2008) and Yamasaki et al. (2008) found similar results for ENSO in a broader area. The mechanisms by which the studied climate variability modes interact with northern South America primarily involve atmospheric transport and circulation processes, as evidenced by their stronger causal influence on rainfall and VIMF. As previous works also established (Trenberth and Shea 2005; Berg et al. 2015; Morales et al. 2017; Duque-Gardeazabal et al. 2024; Ruiz-Vásquez et al. 2024), candidate mechanisms include land-atmosphere interactions such as soil moisture-temperature feedbacks, topographic effects related to the complex Andean orography, and radiative processes influenced by cloud cover, vegetation, or aerosols. Additionally, mesoscale circulation patterns and regional phenomena such as low-level jet systems may contribute to shaping temperature dynamics independently of large-scale ocean-atmosphere variability. At first glance, this result might seem unexpected because T2M exhibits the strongest overall influence on the net $T_{Y \to X}$. However, the usefulness of measuring the relative information flow rate is evident, as it disaggregates the dynamic contribution of a specific climate index regarding the net rate of information flow on the target variable T2M.

Centrality, closeness, and betweenness analyses are useful for highlighting the regions critical for the transfer of information in the study area. The Andes are widely recognized for their significance in terms of biodiversity and ecosystem services. Based on network properties analysis, we conclude that the Tropical Andes also play a predominant role in the connectivity and betweenness of climate variability driven by global climate phenomena, functioning as a dynamic hub within the climate network. This centrality suggests that the Andes may mediate the transfer of information or energy between distinct climatic regions. These findings underscore the topographic and climatic complexity of the Andes in shaping regional teleconnection structures. These results carry important implications for both climate science and environmental management. The central role of the Tropical Andes in the climate network suggests that this region may be especially sensitive to shifts in global climate drivers and downstream impacts. Recognizing the Andes as a dynamic mediator of teleconnections also reinforces the need to align climate resilience strategies with conservation efforts, particularly in areas where biodiversity hotspots and key climate pathways intersect, prioritizing climate monitoring and early warning systems.

The Pacific Oceanic region, which exhibits high connectivity in ENSO-related networks, underscores the robustness of ENSO's influence on regional climate connectivity. The convergence of centrality measures across multiple indices in this area

affirms its well-established role in modulating tropical atmospheric circulation and hydrological patterns across northern South America. These results are consistent with the spatial imprint of Pacific sea surface temperature (SST) anomalies, particularly those associated with the Niño 3 and Niño 3.4 regions, which act as primary drivers of convective activity and large-scale circulation shifts that influence precipitation over Colombia and adjacent areas (Ruiz-Vásquez et al. 2024; Posada-Marín et al. 2023; Cai et al. 2020; Hoyos et al. 2019; Poveda et al. 2011; Tootle et al. 2008; Poveda et al. 2006).

Finally, the connectivity patterns of ocean-driven climate variability in Colombia reveal a hybrid network structure characterized by high clustering and low eccentricity alongside hub regions. However, the lack of conformity to canonical distributions indicates that these climate networks possess a distinctive structural complexity that cannot be fully captured by standard network typologies, which is in agreement with previous climate network works such as Tsonis and Swanson (2008) and Yamasaki et al. (2008).

These results corroborate established climate dynamics and open new avenues for exploring less-understood interactions. Future work should assess the sensitivity of these networks to threshold selection and temporal evolution, as well as explore the predictive potential of these spatial patterns for forecasting regional climate anomalies. Together, these insights deepen our understanding of tropical climate dynamics and highlight the potential of causal network methods to support more targeted climate monitoring and adaptation strategies.

Acknowledgements. The Universidad de Antioquia supported NRP through the Estudiante Instructor program for master's students. IH would like to acknowledge support from the ICTP through the Associates Programme (2026-2031).

Declarations

- **Funding**: NRP was supported by the Universidad de Antioquia through the Estudiante Instructor program for master's students. IH and BR were funded by the Colombian General Royalty System (project InnoMalarIA, BPIN 2024000100086).
- **Conflict of interest**: The authors declare no conflicts of interest.
- **Consent for publication**: All authors have given their consent for publication.
- **Data availability**: All data used in this research are open source and can be found at NOAA Climate Prediction Center and ECMWF Climate Data Store.
- **Code availability**: The source code for this study is available at https://github.com/nicolerivera1/colombian-teleconnections
- **Author contribution**: NRP: writing, conceptualization, data analysis, visualization, and software. IH: writing, conceptualization, methodology, investigation, and supervision. FD: methodology and supervision. BR: conceptualization, methodology, investigation, and supervision.

Appendix A Node-grid correspondece

Nodes are arbitrarily labeled according to regional boundaries, from northeast (NE) to southwest (SW). This map-to-node encoding enables translation from the abstract network representation to the spatial layout of the corresponding map and vice versa.

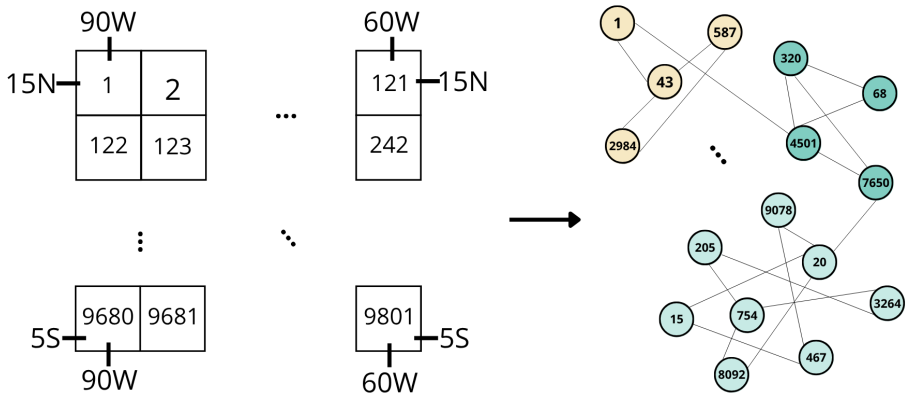


Fig. A1 Node-grid correspondence. Nodes correspond to grid cells in the study area. Links capture the dynamical influence of each global variability mode on the regional climate state.

Appendix B Complementary sources of climate varibility

Appendix Figures B2 and B3 present the spatial distributions of correlation, LKIF, and normalized LKIF associated with the Niño3 and SOI indices, complementing the analysis discussed in the main text.

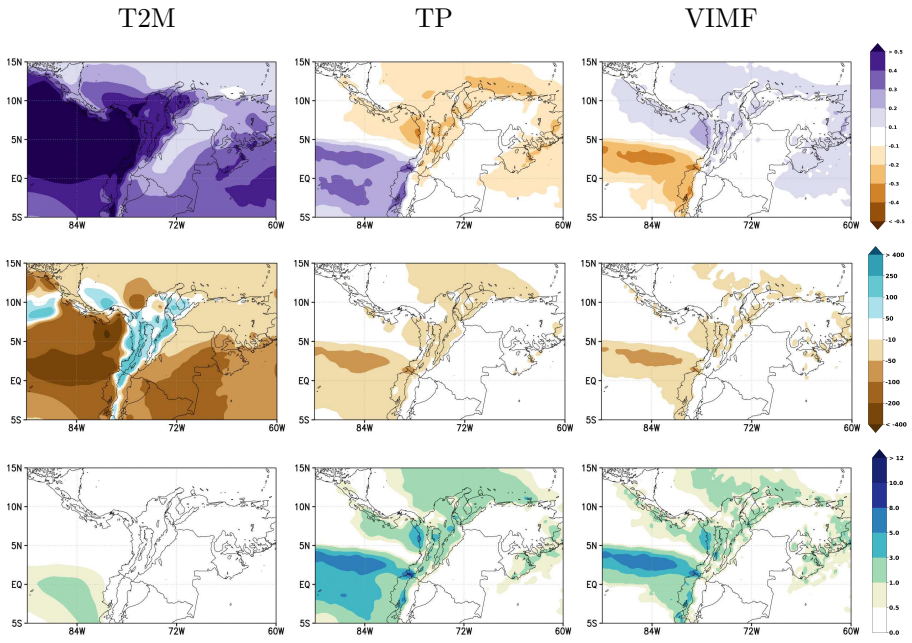


Fig. B2 Influence of Niño 3 index on T2M, TP, and VIMF measured by correlation (top row), LKIF (middle row, in milinats per month), and normalized LKIF (bottom row, in %).

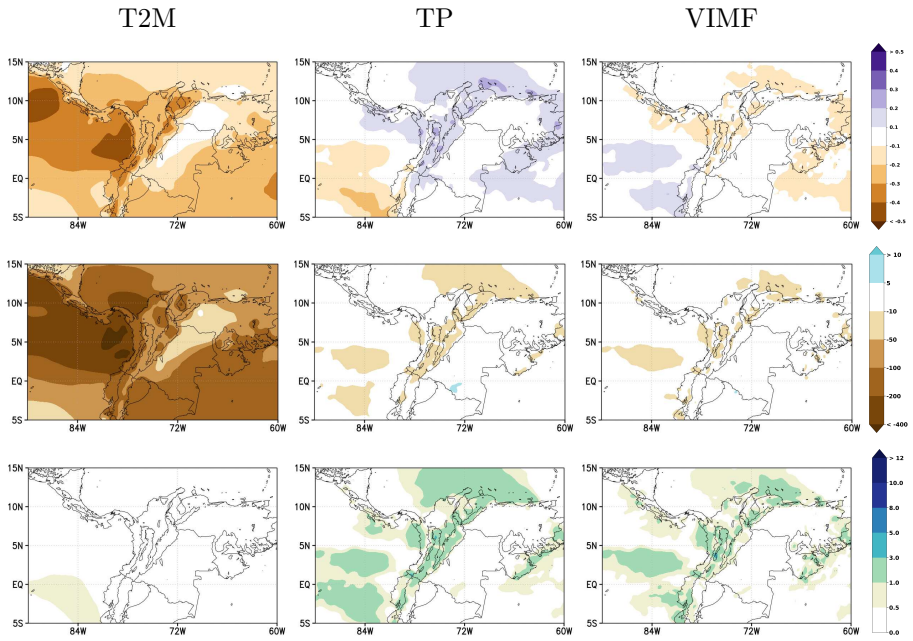


Fig. B3 Influence of SOI index on T2M, TP, and VIMF measured by correlation (top row), LKIF (middle row, in milinats per month), and normalized LKIF (bottom row, %).

The comparison between correlation and LKIF further highlights regions where deterministic ENSO-driven relationships are weak in terms of linear association but remain dynamically connected through causal interactions. The normalized LKIF fields additionally emphasize the spatially heterogeneous contribution of ENSO to regional climate variability, particularly over hydroclimatically sensitive regions. Although the SOI index exhibits a comparatively stronger enhancement of unpredictability over southeastern Colombia, the overall spatial organization of ENSO influence remains coherent across indices, supporting the interpretation of a stable large-scale tropical teleconnection structure governing precipitation and moisture transport variability over northern South America.

Appendix Figures B4 and B5 provide complementary spatial representations of correlation, LKIF, and normalized LKIF associated with the NTA and CAR indices, extending the analysis of Atlantic-driven teleconnections discussed in the main text.

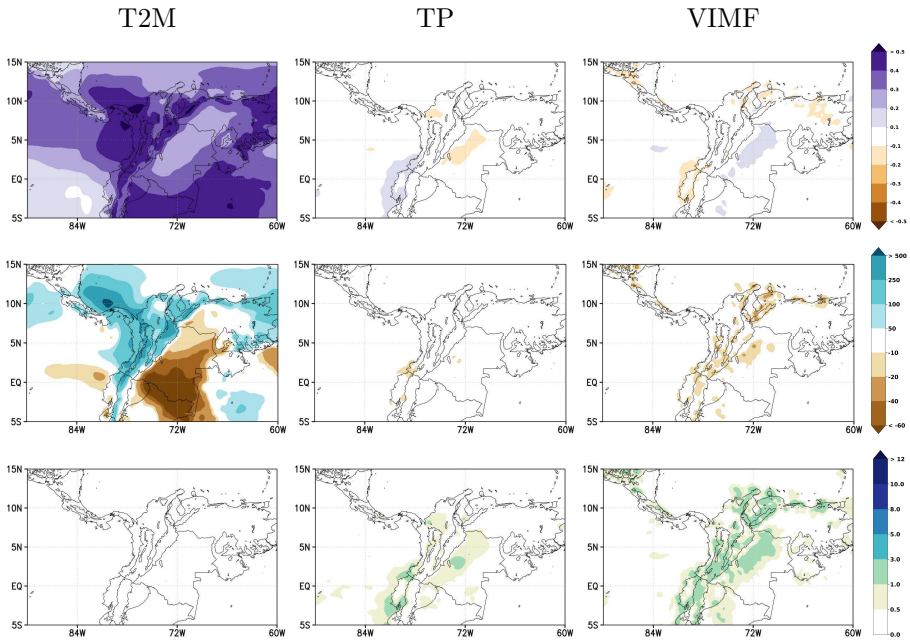


Fig. B4 Influence of NTA index on T2M, TP, and VIMF measured by correlation (top row), LKIF (middle row, in milinats per month), and normalized LKIF (bottom row, in %).

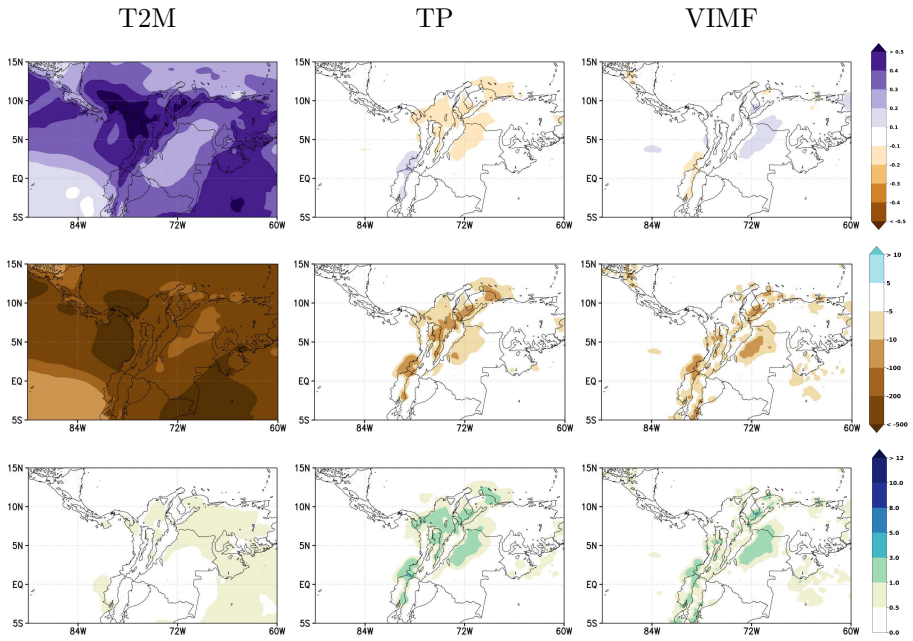


Fig. B5 Influence of CAR index on T2M, TP, and VIMF measured by correlation (top row), LKIF (middle row, in milinats per month), and normalized LKIF (bottom row, in %).

In agreement with the TNA patterns, the NTA index exhibits broader regions of positive LKIF for T2M, indicating a more spatially extensive deterministic teleconnection despite its limited relative contribution to total variability. By contrast, the CAR index is characterized by weaker and predominantly negative LKIF structures, particularly near the Caribbean coast and Amazon basin, suggesting that Atlantic Caribbean variability may enhance stochasticity and reduce predictability in regional temperature fields. These contrasting LKIF signatures among Atlantic indices highlight the heterogeneous nature of Atlantic teleconnections and suggest that distinct Atlantic modes may influence regional climate through different dynamical pathways. Despite these differences, the normalized LKIF values remain generally low, reinforcing the interpretation that Atlantic variability plays a secondary role in explaining regional TP and VIMF variability when compared to ENSO-related forcing.

Appendix C Adjacency matrices

Adjacency matrix representation of networks. Black points represent the links between nodes. These square matrices cover the entire study area with 9801 nodes.

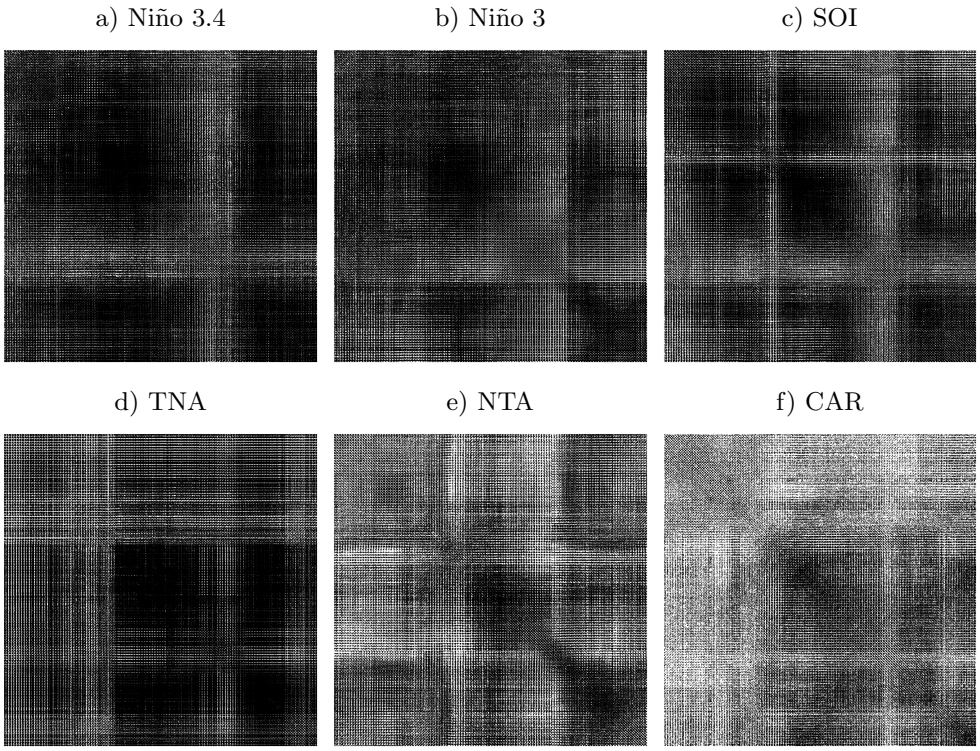


Fig. C6 Adjacency matrix representation for all networks. The dimension is 9801×9801 ($N \times N$), and black points represent links.

Appendix D Eigenvector Centrality

In addition to degree centrality, eigenvector centrality emphasizes the importance of a node's connections by accounting for both the number and the influence of its linked nodes. Both degree (Fig. 5) and eigenvector (D7) centrality reveal a similar spatial structure across the study area, with only minor differences. For example, although the NTA exhibits low maximal degree values, its connections play a crucial role in the overall network structure, particularly in the valleys surrounding the Andes, which appear to facilitate significant information transfer related to associated variability phenomena. Regions with high maximal degree values in the TNA also display high eigenvector centrality, reinforcing their importance within the network. Furthermore, all ENSO-related indices present comparable eigenvector centrality patterns, suggesting that the quantity and influence of connections in these networks preserve a consistent topological structure. This is a notable finding, as it implies that regardless of the specific ENSO index used, the causal network topology influencing Colombia remains stable over the Andean mountain range. Minor differences over the Pacific Cold Tongue across these indices may indicate subtle variations in the pathways of information transfer.

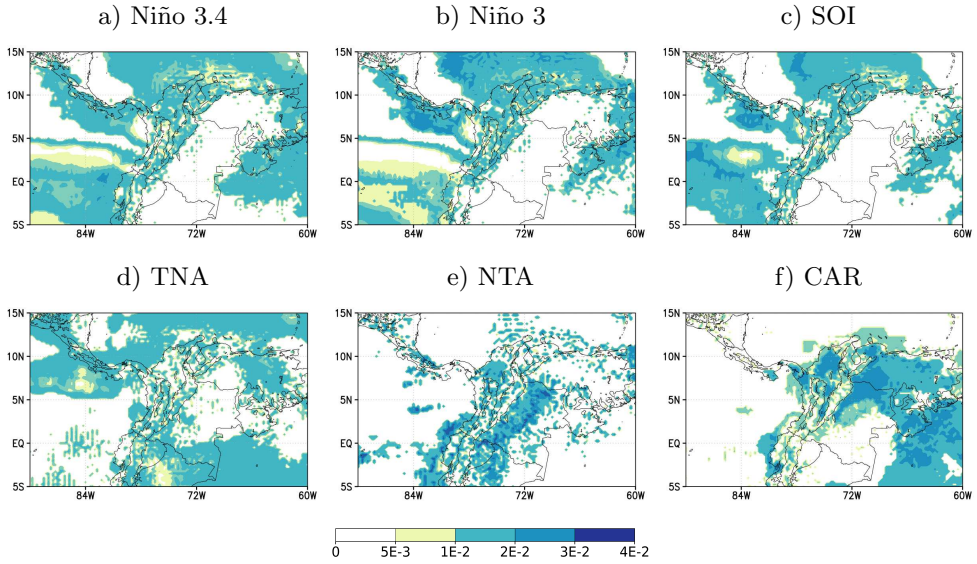


Fig. D7 Eigenvector centrality maps. Higher values indicate higher structural importance.

References

Aceituno P (1988) On the functioning of the Southern Oscillation in the South American sector. Part I: Surface climate. Mon Weather Rev 116(3):505–524. https://doi.org/10.1175/1520-0493(1988)116⟨0505:OTFOTS⟩2.0.CO;2

Aldana-Domínguez J, Montes C, Martínez M, et al (2017) Biodiversity and ecosystem services knowledge in the Colombian Caribbean: progress and challenges. Trop Conserv Sci 10:1940082917714229. https://doi.org/10.1177/19400829177142

Arias PA, Martínez JA, Vieira SC (2015) Moisture sources to the 2010–2012 anomalous wet season in northern South America. Clim Dyn 45:2861–2884. https://doi.org/10.1arias20007/s00382-015-2511-7

Arias PA, Garreaud R, Poveda G, et al (2021) Hydroclimate of the Andes part II: Hydroclimate variability and sub-continental patterns. Front Earth Sci 8:666. https://doi.org/10.3389/feart.2020.505467

Arias PA, Rendón ML, Martínez JA, et al (2023) Changes in atmospheric moisture transport over tropical South America: An analysis under a climate change scenario. Clim Dyn 61(11):4949–4969. https://doi.org/10.1007/s00382-023-06833-4

Barabási AL, Pósfai M (2016) Network science, vol 3. Cambridge University Press

Barrat A, Barthelemy M, Vespignani A (2008) Dynamical processes on complex networks. Cambridge University Press, https://doi.org/10.1017/CBO9780511791383

Bass MS, Finer M, Jenkins CN, et al (2010) Global conservation significance of Ecuador's Yasuní National Park. PloS One 5(1):e8767. https://doi.org/10.1371/journal.pone.0008767

Berg A, Lintner BR, Findell K, et al (2015) Interannual coupling between summertime surface temperature and precipitation over land: Processes and implications for climate change. J Climate 28(3):1308–1328. https://doi.org/10.1175/JCLI-D-14-00324.1

Boccaletti S, Latora V, Moreno Y, et al (2006) Complex networks: structure and dynamics. Phys Rep 424(4-5):175–308. https://doi.org/10.1016/j.physrep.2005.10.009

Botero H, Barnes AP (2022) The effect of ENSO on common bean production in Colombia: A time series approach. Food Secur 14(6):1417–1430. https://doi.org/10.1007/s12571-022-01290-z

Builes-Jaramillo A, Valencia J, Salas HD (2023) The influence of the El Niño-Southern Oscillation phase transitions over the northern South America hydroclimate. Atmos Res 290:106786. https://doi.org/10.1016/j.atmosres.2023.106786

Cai W, Wu L, Lengaigne M, et al (2019) Pantropical climate interactions. Science 363(6430):eaav4236. https://doi.org/10.1126/science.aav42

Cai W, McPhaden MJ, Grimm AM, et al (2020) Climate impacts of the El Niño-Southern Oscillation on South America. Nat Rev Earth Environ 1(4):215–231. https://doi.org/10.1038/s43017-020-0040-3

Canchala T, Alfonso-Morales W, Cerón WL, et al (2020) Teleconnections between monthly rainfall variability and large-scale climate indices in southwestern Colombia. Water 12(7):1863. https://doi.org/10.3390/w12071863

Cohen R, Havlin S (2010) Complex networks: Structure, robustness and function. Cambridge University Press, New York

Cordoba-Machado S, Palomino-Lemus R, Gamiz-Fortis SR, et al (2015) Assessing the impact of El Niño Modoki on seasonal precipitation in Colombia. Glob Planet Change 124:41–61. https://doi.org/10.1016/j.gloplacha.2014.11.003

Deza JI (2015) Climate networks constructed by using information-theoretic measures and ordinal time-series analysis. PhD thesis, Universitat Politècnica de Catalunya, https://doi.org/10.5821/dissertation-2117-95633

Deza JI, Ihshaish H (2015) The construction of complex networks from linear and nonlinear measures–Climate Networks. Procedia Comput Sci 51:404–412. https://doi.org/10.1016/j.procs.2015.05.260

Díaz-Granados Ortiz MA, Navarrete González JD, Suárez López T (2005) Páramos: Hidrosistemas sensibles. Revista de ingeniería (22):64–75. https://doi.org/10.16924/revinge.22.8

Dijkstra HA, Hernández-García E, Masoller C, et al (2019) Networks in climate. Cambridge University Press, https://doi.org/10.1017/9781316275757

Docquier D, Di Capua G, Donner RV, et al (2024) A comparison of two causal methods in the context of climate analyses. Nonlinear Processes in Geophysics 31(1):115–136. https://doi.org/10.5194/npg-31-115-2024

Donges JF, Heitzig J, Beronov B, et al (2015) Unified functional network and nonlinear time series analysis for complex systems science: The pyunicorn package. Chaos 25(11). https://doi.org//10.1063/1.4934554

Donner R, Barbosa S, Kurths J, et al (2009) Understanding the Earth as a Complex System–recent advances in data analysis and modelling in Earth sciences. Eur Phys J Spec Top 174:1–9. https://doi.org/10.1140/epjst/e2009-01086-6

Donner RV, Wiedermann M, Donges JF (2017) Complex network techniques for climatological data analysis. In: Franzke CLE, O'Kane TJ (eds) Nonlinear and Stochastic

Climate Dynamics. Cambridge University Press, p 159–183

Duque-Gardeazabal N, Friedman AR, Brönnimann S (2024) An atlantic influence on evaporation in the orinoco and amazon basins. EGU Sphere Preprint https://doi.org/10.5194/egusphere-2024-2846

Escobar M, Hoyos I, Nieto R, et al (2022) The importance of continental evaporation for precipitation in Colombia: A baseline combining observations from stable isotopes and modelling moisture trajectories. Hydrol Process 36(6):e14595. https://doi.org/10.1002/hyp.14595

Espinoza JC, Garreaud R, Poveda G, et al (2020) Hydroclimate of the andes Part I: Main climatic features. Front Earth Sci 8:64. https://doi.org/10.3389/feart.2020.00064

Fortunato S (2010) Community detection in graphs. Phys Rep 486(3-5):75–174. https://doi.org/10.1016/j.physrep.2009.11.002

Froyland G, Stuart RM, van Sebille E (2014) How well-connected is the surface of the global ocean? Chaos 24(3):033126. https://doi.org/10.1063/1.4892530

Golbeck J (2015) Introduction to social media investigation: A hands-on approach. Elsevier Inc

Grimm AM, Tedeschi RG (2009) ENSO and extreme rainfall events in South America. J Climate 22(7):1589–1609. https://doi.org/10.1175/2008JCLI2429.1

Hersbach H, Bell B, Berrisford P, et al (2020a) The ERA5 Global Reanalysis: Achieving a detailed record of the climate and weather for the past 70 years. EGU Gen Assem 2020 10375. https://doi.org/10.5194/EGUSPHERE-EGU2020-10375

Hersbach H, Bell B, Berrisford P, et al (2020b) The ERA5 global reanalysis. Q J R Meteorol Soc 146(730):1999–2049. https://doi.org/10.1002/qj.3803

Hoyos I, Rodríguez BA (2020) Drawing the complexity of Colombian climate from non-extensive extreme behavior. Physica A 548:123673. https://doi.org/10.1016/j.physa.2019.123673

Hoyos I, Baquero-Bernal A, Jacob D, et al (2013) Variability of extreme events in the Colombian Pacific and Caribbean catchment basins. Clim Dyn 40:1985–2003. https://doi.org/10.1007/s00382-012-1487-9

Hoyos I, Dominguez F, Cañón-Barriga J, et al (2018) Moisture origin and transport processes in Colombia, northern South America. Clim Dyn 50:971–990. https://doi.org/10.1007/s00382-017-3653-6

Hoyos I, Cañón-Barriga J, Arenas-Suárez T, et al (2019) Variability of regional atmospheric moisture over northern South America: Patterns and underlying phenomena.

Clim Dyn 52:893–911. https://doi.org/10.1007/s00382-018-4172-9

IDEAM (2005) Atlas climatológico de Colombia. Instituto de Hidrología, Meteorología y Estudios Ambientales, Bogotá

Jönsson BF, Follett CL, Bien J, et al (2023) Using probability density functions to evaluate models (pdfem, v1. 0) to compare a biogeochemical model with satellite-derived chlorophyll. Geosci Model Dev 16(16):4639–4657. https://doi.org/10.5194/gmd-16-4639-2023

Kousky VE, Kagano MT, Cavalcanti IFA (1984) A review of the southern oscillation: oceanic-atmospheric circulation changes and related rainfall anomalies. Tellus A 36A(5):490–504. https://doi.org/10.1111/j.1600-0870.1984.tb00264.x

Lee H, Calvin K, Dasgupta D, et al (2023) IPCC, 2023: Summary for Policymakers. In: Climate Change 2023: Synthesis Report. Contribution of Working Groups I, II and III to the Sixth Assessment Report of the Intergovernmental Panel on Climate Change. Intergovernmental Panel on Climate Change (IPCC), https://doi.org/10.59327/IPCC/AR6-9789291691647.001

Liang XS (2008) Information flow within stochastic dynamical systems. Phys Rev E 78(3):031113. https://doi.org/10.1103/PhysRevE.78.031113

Liang XS (2014) Unraveling the cause-effect relation between time series. Phys Rev E 90(5):052150. https://doi.org/10.1103/PhysRevE.90.052150

Liang XS (2015) Normalizing the causality between time series. Phys Rev E 92:022126. https://doi.org/10.1103/PhysRevE.92.022126

Liang XS (2016) Information flow and causality as rigorous notions ab initio. Phys Rev E 94(5):052201. https://doi.org/10.1103/PhysRevE.94.052201

Liang XS (2018) Causation and information flow with respect to relative entropy. Chaos 28(7). https://doi.org/10.1063/1.5010253

Lozano-Durán A, Arranz G (2022) Information-theoretic formulation of dynamical systems: Causality, modeling, and control. Phys Rev Res 4:023195. https://doi.org/10.1103/PhysRevResearch.4.023195

Majda AJ, Harlim J (2007) Information flow between subspaces of complex dynamical systems. PNAS 104(23):9558–9563. https://doi.org/10.1073/pnas.0703499104

Mesa S OJ, Poveda J G, Carvajal S LF (1997) Introducción al clima de Colombia. Universidad Nacional de Colombia

Morales J, Arias P, Martínez J (2017) Role of caribbean low-level jet and choco jet in the transport of moisture patterns towards central america. In: Proceedings of First International Electronic Conference on the Hydrological Cycle. MDPI, CHyCle, p

733 4861, https://doi.org/10.3390/chycle-2017-04861

734 Myers N, Mittermeier RA, Mittermeier CG, et al (2000) Biodiversity hotspots for con-
735 servation priorities. Nature 403(6772):853–858. https://doi.org/10.1038/35002501

736 Negre CF, Morzan UN, Hendrickson HP, et al (2018) Eigenvector centrality for char-
737 acterization of protein allosteric pathways. PNAS 115(52):E12201–E12208. https:
738 //doi.org/10.1073/pnas.1810452115

739 Newman M (2002) The structure and function of networks. Comp Phys Commun
740 147(1–2):40–45. https://doi.org/10.1016/s0010-4655(02)00201-1

741 Newman M (2018) Networks. Oxford University Press, New York, https://doi.org/10.
742 1093/oso/9780198805090.001.0001

743 Newman M, Barabási AL, Watts DJ (2011) The structure and dynamics of networks.
744 Princeton University Press

745 Pabón-Caicedo JD, Arias PA, Carril AF, et al (2020) Observed and projected hydro-
746 climate changes in the Andes. Frontiers in Earth Science 8:61. https://doi.org/10.
747 3389/feart.2020.00061

748 Posada-Marín JA, Arias PA, Jaramillo F, et al (2023) Global impacts of El Niño
749 on terrestrial moisture recycling. Geophys Res Lett 50(10):e2023GL103147. https:
750 //doi.org/10.1029/2023GL103147

751 Poveda G, Waylen PR, Pulwarty RS (2006) Annual and inter-annual variability of the
752 present climate in northern South America and southern Mesoamerica. Palaeogeogr
753 Palaeoclimatol Palaeoecol 234(1):3–27. https://doi.org/10.1016/j.palaeo.2005.10.
754 031

755 Poveda G, Álvarez DM, Rueda ÓA (2011) Hydro-climatic variability over the Andes
756 of Colombia associated with ENSO: a review of climatic processes and their impact
757 on one of the Earth's most important biodiversity hotspots. Clim Dyn 36(11):2233–
758 2249. https://doi.org/10.1007/s00382-010-0931-y

759 Poveda G, Espinoza JC, Zuluaga MD, et al (2020) High impact weather events in the
760 Andes. Front Earth Sci 8:162. https://doi.org/10.3389/feart.2020.00162

761 Rehbein A, Ambrizzi T (2023) ENSO teleconnections pathways in South America.
762 Clim Dyn 61(3):1277–1292. https://doi.org/10.1007/s00382-022-06624-3

763 Ruiz-Vásquez M, Arias PA, Martínez JA (2024) Enso influence on water vapor trans-
764 port and thermodynamics over northwestern south america. Theor Appl Clim
765 155(5):3771–3789. https://doi.org/10.1007/s00704-024-04848-3

766 Sánchez-Cuervo AM, Aide TM, Clark ML, et al (2012) Land cover change in Colombia:
767 Surprising forest recovery trends between 2001 and 2010. PLoS ONE 7(8):e43943.

https://doi.org/10.1371/journal.pone.0043943

Sanderson M, fox C, Hodge K, et al (2022) Impacts of the ENSO cycle on climate and coffee production in Colombia. EGU Gen Assem 2022 https://doi.org/10.5194/egusphere-egu22-13513

Serrão EA, Cavalcante RB, Zanin PR, et al (2025) The effects of teleconnections on water and carbon fluxes in the two South America's largest biomes. Sci Rep 15(1):1395. https://doi.org/10.1038/s41598-025-85272-z

Sethna JP (2021) Statistical mechanics: entropy, order parameters, and complexity. Oxford University Press, USA

Souza ED, Ambrizzi T (2002) ENSO impacts on the South American rainfall during 1980s: Hadley and Walker circulation. Atmósfera 15(2):105–120

Stanley HE (1999) Scaling, universality, and renormalization: Three pillars of modern critical phenomena. Rev Mod phys 71(2):S358. https://doi.org/10.1103/RevModPhys.71.S358

Steinhaeuser KJK, Chawla N, Ganguly AR (2010) Complex networks in climate science: Progress, opportunities and challenges. National Center for Computational Sciences (NCCS), pp 16–26, URL https://www.osti.gov/biblio/1023819

Takaya Y, Ganeshi NG, Kosaka Y, et al (2025) Influence of soil moisture on surface air temperature in monsoons. Geophysical Research Letters 52(20). https://doi.org/10.1029/2025gl115760, URL http://dx.doi.org/10.1029/2025GL115760

Tawia Hagan DF, Wang G, San Liang X, et al (2019) A time-varying causality formalism based on the liang–kleeman information flow for analyzing directed interactions in nonstationary climate systems. J Clim 32(21):7521–7537. https://doi.org/10.1175/JCLI-D-18-0881.1

Tootle GA, Piechota TC, Gutiérrez F (2008) The relationships between Pacific and Atlantic Ocean sea surface temperatures and Colombian streamflow variability. J Hydrol 349(3–4):268–276. https://doi.org/10.1016/j.jhydrol.2007.10.058

Trenberth KE, Shea DJ (2005) Relationships between precipitation and surface temperature. Geophys Res Lett 32(14). https://doi.org/10.1029/2005GL022760

Tsonis AA, Roebber PJ (2004) The architecture of the climate network. Physica A 333:497–504. https://doi.org/10.1016/j.physa.2003.10.045

Tsonis AA, Swanson KL (2008) Topology and predictability of El Niño and La Niña networks. Phys Rev lett 100(22):228502. https://doi.org/10.1103/PhysRevLett.100.228502

802 Tsonis AA, Swanson KL, Roebber PJ (2006) What do networks have to do with
803 climate? BAMS 87(5):585–596. https://doi.org/10.1175/BAMS-87-5-585

804 Tsonis AA, Swanson KL, Wang G (2008) On the role of atmospheric teleconnections
805 in climate. J Clim 21(12):2990–3001. https://doi.org/10.1175/2007JCLI1907.1

806 Urrea V, Ochoa A, Mesa O (2019) Seasonality of rainfall in Colombia. Water Resour
807 Res 55(5):4149–4162. https://doi.org/10.1029/2018WR023316

808 Waylen P, Poveda G (2002) El niño–southern oscillation and aspects of western south
809 american hydro-climatology. Hydrol Process 16(6):1247–1260. https://doi.org/10.
810 1002/hyp.1060

811 West BJ, Scafetta N (2010) Disrupted networks: from physics to climate change. World
812 Scientific

813 Wilks DS (2019) Statistical methods in the atmospheric sciences, 4th edn. Elsevier
814 Science Publishing, Philadelphia, PA

815 Xu J (2001) Interconnection Networks and Graphs, Springer US, p 1–38. https://doi.
816 org/10.1007/978-1-4757-3387-7_1

817 Yamasaki K, Gozolchiani A, Havlin S (2008) Climate networks around the globe are
818 significantly affected by El Niño. Phys Rev Lett 100(22):228501. https://doi.org/
819 10.1103/PhysRevLett.100.228501